JOURNAL OF GEOPHYSICAL RESEARCH, VOL. 101, NO. C2, PAGES 3801–3816, FEBRUARY 15, 1996

Assimilation of wave data into the wave model WAM using an impulse response function method

E. Bauer,[1] K. Hasselmann,[2] I. R. Young,[3] and S. Hasselmann[2]

Abstract. A new method for the assimilation of wave data into a third-generation wave model is presented. Deviations between observed and modeled wave spectra are used to derive corrections of the wind field which drives the wave model. The wave field can then be subsequently corrected by a new integration of the wave model with the improved wind field. A basic difficulty of such dynamically consistent wave data assimilations schemes which correct both wind and wave data is the nonsynchronous and nonlocal nature of the wind field corrections: errors observed in the wave spectrum at a given measurement time and location can be produced by errors in the wind field at much earlier times and far distant locations. Formally, these problems can be rigorously resolved by the adjoint modeling method. However, in practice, the adjoint technique requires an order of magnitude more computer time than the integration of the wave model itself. Here an alternative method is developed. The linearized wave model equation which relates small wind to wave spectrum changes is inverted. The central assumption of the inversion is that the wind impact functions representing the impulse response (Green's) function of the wave evolution can be approximated by a δ-function. Physically, this implies that the wind field perturbations responsible for observed perturbations in the wave spectrum can be regarded as strongly localized in space and time for any given component of the spectrum. To obtain stable estimates, the corrections for different wave components are averaged over wavenumber clusters representing different wave systems. For cases in which the linear approximation is inadequate, the method can be applied iteratively. Tests of the concept and application of the method for a number of synthetic wind field cases are encouraging.

1. Introduction

In recent years, significant progress has been achieved in our understanding of the mechanisms responsible for the generation and evolution of ocean wind waves and in our ability to implement these advances in numerical wave models. In the latest third-generation wave models the energy balance equation is now solved for the first time by direct integration of the physical source function, without any predefined constraints on the spectral shape. The first such wave model WAM is now used at a large number of research institutes and operational forecasting centers. It has been shown in many independent intercomparison studies to yield reliable results [*WAMDI Group,* 1988; *Zambresky,* 1989; *Romeiser,* 1993; *Cardone et al.*, 1995; *Komen et al.*, 1994].

In a global wave hindcast study using altimeter data of the satellite Seasat, however, the agreement between the WAM model and observed wave heights was found to be poorer in the southern than in the northern hemisphere [*Hasselmann et al.*, 1988; *Bauer et al.*, 1992; see also *Romeiser,* 1993]. Most of the errors could be attributed to inaccuracies in the forcing surface stress fields. The studies demonstrated the sensitivity of wave models to the input wind fields (which follows from the approximately quadratic dependence of the wave height on the wind speed) and thus the potential value of wave models as a tool for the quality assurance and correction of wind field data.

Recently, both wind and wave data have become available globally, continuously and in near real time through ERS-1 and ERS-2 (and in an off-line mode through TOPEX/POSEIDON). It is anticipated that these data will continue to be provided in near real time in the future by a series of polar platforms and special satellites such as ADEOS and SARSAT. To make full use of this new information, methods must be developed for assimilating these data in real time into global wave

[1] Institut für Meereskunde, Universität Hamburg, Hamburg, Germany.

[2] Max-Planck-Institut für Meteorologie, Hamburg, Germany.

[3] Department of Civil and Maritime Engineering, University College, University of New South Wales , Canberra, Australia.

Paper number 95JC03306.
0148-0227/96/95JC-03306$05.00

models such as WAM in order to provide dynamically consistent analyses of both wind and wave fields.

The accuracy of the wind and wave corrections derived from such assimilation methods will necessarily depend on the quality of the wave models. Errors in the model dynamics will produce errors in the analyzed fields. In the case of the WAM model, extensive verification studies [*Komen et al.*, 1994] indicate that the model has reached a sufficient level of maturity that the wind field corrections derived by the assimilation of wave data into the model should be operationally useful. However, the value of dynamical data assimilation is not governed simply by the quality of the models. Assimilation techniques should be viewed, rather, as tools to jointly assess the quality of data and models in a dynamically consistent framework. To identify shortcomings in the representation of the physical processes in models of complex dynamical systems, many different measurements are generally needed. The only effective technique for analyzing the dynamical implications of such different sources of data, with consideration both to the structure of the model and the limitations of the data, is data assimilation.

Preliminary attempts to assimilate wave data into wave models have been described by *Komen* [1985], *Thomas* [1988], *Janssen et al.* [1989], *Bauer et al.* [1992], and *Lionello et al.* [1992].

These schemes have generally emphasized the use of measurements of the wave field to directly modify the wave field, without systematically correcting the analyzed wind field except (in some cases) in an ad hoc manner at the measurement point. Although such techniques yield some improvement of the wave model predictions, they basically address the symptom of the problem (the waves), rather than the cause (the wind).

Ideally, a scheme is required which uses measured wave data to correct the wind field, thereby also providing a dynamically consistent correction of the wave field through a subsequent integration of the wave model with the corrected winds. This paper presents such a technique. It employs the WAM model to infer the corrections which need to be applied to the input wind field to minimize the difference between the observed and model wave data. The approach may be regarded as a first step toward a more comprehensive system in which both wave and wind data, either from satellite sensors or from conventional measurement networks, are assimilated simultaneously into global wave models and atmospheric weather prediction models.

The success of such an integrated assimilation scheme depends, of course, ultimately on the ability of the wave model to reproduce the dynamics of the observed wave field. The modified wind fields will be correct only if the wave model is correct. Although the WAM model represents a significant advance over earlier first- and second-generation wave models in the explicit representation of the wave physics, the model will undoubtedly still contain errors which will lead to systematic errors in the corrected wind fields. However, the development of wave models and wave data assimilation schemes should be regarded as an iterative, coupled enterprise. Only through the experience gained from the application of wave data assimilation schemes will it be possible to exploit the wealth of information provided by modern satellite systems to identify and correct shortcomings in wind and wave models and the associated data assimilation schemes.

The paper is organized as follows: Experience gained from the preliminary assimilation studies is briefly discussed in section 2. In section 3 the general forms of the cost function and the impulse response (Green's) function approach are introduced. The implementation of the δ-function approximation for the wind impact functions is presented in section 4, together with the associated determination of the wave age. The numerical implementation uses an analytical integration scheme described in section 5. Free parameters of the Green's function scheme are adjusted using a conjugate gradient algorithm described in section 6. Application studies of the assimilation scheme in different synthetic sea state conditions are presented in section 7. The results are summarized and the anticipated performance in real applications is discussed in the concluding section 8.

2. Wave Data Assimilation Techniques

One of the first published attempts to assimilate wave height data in a wave prediction model was made by *Komen* [1985]. He investigated swell propagating from a generation region in the Norwegian Sea to a measurement point at the entrance of Rotterdam harbor. The prediction of the swell at Rotterdam harbor for this event using the Golven Nordzee (GONO) model [*Janssen et al.*, 1984] was significantly higher than measured. Updating the model with measured buoy data at a point approximately 500 km north of the measurement site significantly improved the model swell prediction.

Thomas [1988] proposed the first scheme to update the full wave spectrum using buoy measurements of significant wave height and wind speed. A Joint North Sea Wave Project (JONSWAP) parameterization [*Hasselmann et al.*, 1973] was assumed for the wind sea part of the spectrum, which was then updated by using the buoy wind speed to rescale the energy and peak frequency (maintaining the so-called wave age, defined as the ratio between the peak phase velocity and wind velocity). The remaining swell part of the spectrum was updated by changing only the energy scale. This technique yielded promising results and demonstrated the basic feasibility of operational wave data assimilation schemes.

Hasselmann et al. [1988] and *Bauer et al.* [1992] made the first attempt at the assimilation of global satellite data using Seasat altimeter wave height data for a 30-day period in August 1978. Their update scheme simply changed the scale of the spectrum,

$$E_{\text{new}}(f,\theta) = \gamma E_{\text{model}}(f,\theta)$$

where $E_{new}(f,\theta)$ is the new or modified spectrum, $E_{model}(f,\theta)$ is the initial model spectrum, f is frequency, and θ is the propagation direction. The scale factor γ at the subsatellite point of the altimeter measurement was set proportional to the square of the ratio between the altimeter wave height and the model first-guess wave height and relaxed back linearly to unity at the boundary of some specified "region of influence". For a continuous 1-month assimilation experiment, good results were achieved using a region of influence of 9° x 9°. The assimilation scheme was successful in updating regions dominated by swell, yielding globally averaged decay times for the swell correction of the order of 5 days, but had little impact on the wind sea, which reverted rather rapidly to an equilibrium corresponding to the uncorrected local wind. It was concluded that the improvement of the wind sea predictions would require a scheme which also corrects the erroneous wind forcing.

This problem was addressed by *Janssen et al.* [1989], who used the altimeter wave height data to introduce corrections to both the wave and wind fields. Their scheme first partitioned the spectrum into wind sea and swell, the swell being defined as the region of the spectrum in which the atmospheric input source term was zero. The swell spectrum was modified by a change of the energy scale, maintaining the spectral shape and peak frequency. The wind sea part of the spectrum was corrected in a manner similar to that of *Thomas* [1988] using JONSWAP-type [*Hasselmann et al.,* 1976] duration limited growth relations. Introducing the additional assumption that the energies of the wind sea and swell were changed by the same factor, new wind sea and swell spectra were then determined. At the same time the wind speed (or friction velocity u_*) was adapted to conform with the new wind sea. This information was then distributed to surrounding grid points, as in the work of *Hasselmann et al.* [1988], but using a correlation region of only one wave model grid square (3° × 3°). Although both the wind and sea state had now been adjusted, only relatively short correction decay times of the order of 1 day were achieved. This was presumably largely due to the much smaller region of influence used. If the scale of the region of influence is significantly smaller than the spacing between successive ascending or descending satellite orbits (~25° longitude), only a small fraction of the ocean is corrected in 1 day's sweep of the satellite over the ocean. Wave energy from uncorrected regions between the satellite tracks can then propagate into the corrected regions and degrade the quality of the updated regions.

Lionello et al. [1992] have proposed a modification of the scheme of *Janssen et al.* [1989] using a large region of influence and alternative scaling relations. When swell leaves a generation region, it initially has a relatively large steepness characteristic of a wind sea. However, linear dispersion and the nonlinear processes of dissipation and energy transfer, both of which are strongly dependent on the wave steepness, rapidly reduce the steepness to a level where all the source terms become negligible. If the wave height is underpredicted by the model (which was normally the case for the Seasat studies), the assimilation schemes mentioned above all increase the swell steepness. This immediately activates the dissipation and nonlinear source terms, causing the wave energy to decrease again. In the rescaling scheme of *Lionello et al.* [1992] both the amplitude and the frequency of the swell were altered such that the swell steepness is maintained during the assimilation process. By this modified method the correction decay times were increased significantly, in the case of swell, up to the order of the ocean-basin traversal times.

The above assimilation schemes are all relatively simple and exhibit a number of shortcomings when implemented in a third-generation wave model. All treat wind sea and swell separately, as in second-generation models, and introduce rather ad hoc assumptions to distribute the correction in the total energy between these two components. This negates one of the major strengths of third-generation wave models, in which such a division is no longer needed, the spectrum being free to respond to the given source functions without prescribing the spectral shape or scales. Finally, the wind update is made only for the local instantaneous wind, although the wave spectrum often represents the nonlocal response to the past wind at a distant location. Furthermore, the significantly higher potential information contained in the remote-sensed spectral wave observations from synthetic aperture radars (SAR) [*Hasselmann and Hasselmann,* 1991; *Brüning et al.,* 1993, 1994] is not included.

A more fundamental approach is clearly called for in which the model predictions are fitted to the observations by modifying the model control variables, i.e., the wind field, rather than the model output. A general solution to this problem is given by the adjoint model formalism [*Marchuk,* 1974; *Le Dimet and Talagrand,* 1986; *Thacker,* 1988]. The basic concept of this approach is to determine changes needed in the control variables to achieve a desired change in the model prediction. Adjoint wave models have been developed and successfully applied to assimilate wave data in individual case studies [*de Valk and Calkoen,* 1989; *de las Heras and Janssen,* 1992] or to optimize the model source functions (*G. Barzel et al.,* manuscript in preparation 1994). However, for global operational implementation with a third-generation wave model the adjoint model approach appears to be computationally very costly.

Formally, the change in the wind field needed to produce a given change in the wave field can be determined by inverting the wave model equation. However, this is normally an even more expensive computation. In fact, the purpose of the adjoint method is to determine the control variable changes needed to achieve a desired change in the model output without explicitly inverting the model equations [cf. *Komen et al.,* 1994]. The adjoint model approach requires successively solving the model equations and adjoint model equations for prescribed source terms in an iterative minimization loop. In contrast, the inversion of the model equations re-

quires the determination of the inverse of the linear system matrix, which for n variables is a roughly n times more costly operation than determining a single solution of the linearized model equations. For large n the number of minimization iterations required for the adjoint approach is normally significantly smaller than n, so that the adjoint method is more efficient than the direct inversion approach. Nevertheless, we explore in the following an alternative assimilation method in which the wave transport equation operator is inverted, but under strongly simplifying assumptions. The basic idea is to estimate the impulse response (Green's) function of the linearized system which describes the response of the spectral energy balance to perturbations in the wind fields. Our central assumption is that the response is strongly localized in space and time.

We shall not address in this paper the full problem of simultaneously assimilating both wind and wave data in an atmospheric weather prediction model and a global wave model. However, the method presented here can, in principle, be readily extended to such a comprehensive data assimilation system.

3. General Structure of the Green's Function Assimilation Approach

We wish to optimally adapt the wave field predicted by a wave model to a finite set of wave measurements. These can represent, e.g., significant wave heights obtained from satellite altimeters; one-dimensional frequency spectra; low directional resolution, two-dimensional spectra measured with buoys; or full two-dimensional spectra inferred from wave arrays, SARs, or other special remote sensing systems. Optimal implies here that the modified wave field should represent a best fit to the observed data under the dynamic constraints of the wave model in a maximum likelihood sense.

The maximum likelihood solution is defined as the set of control parameters which maximizes the joint probability function of the multivariate data distribution. The control parameters in the present case are wind corrections. Assuming the errors of the wave data obey Gaussian statistics, then maximizing the multivariate normal probability function is equivalent to minimizing the first term of the cost function

$$J = (\hat{\boldsymbol{D}} - \boldsymbol{D})^T \boldsymbol{M}^{-1} (\hat{\boldsymbol{D}} - \boldsymbol{D}) + (\hat{\boldsymbol{U}} - \boldsymbol{U})^T \boldsymbol{N}^{-1} (\hat{\boldsymbol{U}} - \boldsymbol{U}) \tag{1}$$

where the vectors $\hat{\boldsymbol{D}}$ and $\boldsymbol{D}$ represent the adjusted and the observed wave data, respectively; $\boldsymbol{M}$ is the error covariance matrix of the observational errors, and the superscript T denotes the transpose. Low values of the costs are achieved for small distances between the improved model data and the observed data, with a distance metric given by the inverse of the data error covariance matrix. The second term of the cost function represents an additional penalty to limit excessively large wind corrections, where $\hat{\boldsymbol{U}}$ and $\boldsymbol{U}$ are the adjusted and the first-guess wind data, respectively, and $\boldsymbol{N}$ is the error covariance of the first-guess wind data. Since $\hat{\boldsymbol{D}}$ is a function of $\hat{\boldsymbol{U}}$ through the wave model, the minimization of (1) defines an optimization problem for the wind velocity field $\hat{\boldsymbol{U}}$.

As the error covariance matrices are normally not well known, we assume that the data errors are uncorrelated. Thus the error covariance matrices are reduced to diagonal forms and the cost function becomes

$$\begin{aligned} J &= \sum_r \left[\left(D_r + d_r - D_r^{\mathrm{obs}} \right)^2 / (\sigma_r)^2 \right] \\ &+ H \sum_p \left\{ \left[u_p^2/(\sigma_p^u)^2 + v_p^2/(\sigma_p^v)^2 \right] \right\} \end{aligned} \tag{2}$$

where D_r^{obs} is the rth observed wave data value; D_r is the corresponding first-guess value inferred from the model; d_r is the modification to this first-guess value after optimization; u_p and v_p are the changes introduced into the x and y components of the wind velocity fields (at locations indicated by the index p); H is a suitably chosen weighting factor and σ_r, σ_p^u, σ_p^v represent the standard deviations of the observed data D_r^{obs} and the first-guess wind data (U, V), respectively. Initially, we shall set $\sigma_p^u = \sigma_p^v = \mathrm{const}$, so that these terms can be incorporated in the common weighting factor H and dropped. While the assumption of uncorrelated errors appears reasonable for wave data, it will not normally apply for the first-guess wind field errors. However, it will be found that this is not critical in the following applications, in which the wind corrections inferred from the wave model are not yet assimilated in an atmospheric model.

From the wave energy balance equation

$$\frac{DE}{Dt} = \frac{\partial E}{\partial t} + \boldsymbol{c}_g \cdot \nabla E = S_t(E, \boldsymbol{U}) \tag{3}$$

where E is the directional wave spectrum, $\boldsymbol{c}_g$ is the wave group velocity, and S_t is the total source function [cf. *WAMDI Group*, 1988]. A linearized relation between a small modification e of the wave spectrum and a small modification $\boldsymbol{u}$ of the friction velocity can be obtained in the form,

$$\frac{De}{Dt} = \frac{\delta S_t}{\delta E} e + \frac{\partial S_t}{\partial \boldsymbol{U}} \cdot \boldsymbol{u} \tag{4a}$$

or

$$Le = \frac{\partial S_t}{\partial \boldsymbol{U}} \cdot \boldsymbol{u} \tag{4b}$$

where $L = (D/Dt - \Lambda)$ with $\Lambda = \delta S_t / \delta E$. The integration of (4b) is obtained formally by inverting the linear operator L

$$e = L^{-1} \left[\frac{\partial S_t}{\partial \boldsymbol{U}} \cdot \boldsymbol{u} \right] \tag{5a}$$

or explicitly for e as function of wavenumber $\boldsymbol{k}$, location $\boldsymbol{x}$ and time t

$$e(\boldsymbol{k}; \boldsymbol{x}, t) =$$

$$\int\int\int G(\boldsymbol{k};\boldsymbol{x},t;\boldsymbol{x}',t')\frac{\partial S_t}{\partial \boldsymbol{U}}\cdot\boldsymbol{u}(\boldsymbol{k};\boldsymbol{x}',t')\,d\boldsymbol{x}'dt' \quad (5b)$$

where $G = L^{-1}$ is the Green's (or impulse response) function for which

$$LG(\boldsymbol{k};\boldsymbol{x},t;\boldsymbol{x}',t') = \delta(\boldsymbol{k};\boldsymbol{x}-\boldsymbol{x}',t-t') \quad (6)$$

[*Roach,* 1982; *Fennel and Lass,* 1989].

In practice, the rigorous implementation of this approach will not be feasible, since the determination of the impulse response function G requires the inversion of the prognostic operator L occurring in the spectral perturbation equation (1b). In discretized form this involves the inversion of a very high dimensional matrix. In the adjoint method the inversion problem is avoided by solving the linearized model equations only for the specific source function perturbations arising in the iterative construction of the optimal solution [cf. *Marchuk,* 1974; *Le Dimet and Talagrand,* 1986]. Even this approach, however, requires multiple integrations of the model and the adjoint model equations and becomes very time-consuming when applied to a full third-generation wave model.

We shall accordingly pursue a direct inversion approach but will attempt to reduce the problem to a computationally tractable level by introducing appropriate simplifications for the impulse response function. Our essential approximation, motivated by the dynamics of the wave field and discussed in section 4, is that for any given spectral perturbation $e(\boldsymbol{k};\boldsymbol{x},t)$ there exists a highly localized region in space and time in which a perturbation $\boldsymbol{u}$ of the wind velocity field is most effective. Thus we assume that the factor in the integrand of (5) which acts on the wind field perturbation $\boldsymbol{u}$, can be approximated by a δ-function,

$$G(\boldsymbol{k};\boldsymbol{x},t;\boldsymbol{x}',t')\frac{\partial S_t}{\partial \boldsymbol{U}} = \delta(\boldsymbol{x}'-\boldsymbol{x}_p)\delta(t'-t_p)\boldsymbol{W}(\boldsymbol{k};\boldsymbol{x},t) \quad (7)$$

where the influence point $(\boldsymbol{x}_p, t_p)$ is a function of $(\boldsymbol{k},\boldsymbol{x},t)$. $\boldsymbol{W} = (W^u, W^v)$ represents the spectral impact function with respect to wind perturbations u, v in the x and the y directions, respectively. Thus the general relation for the spectral energy changes resulting from wind changes simplifies to

$$e(\boldsymbol{k};\boldsymbol{x},t) = W^u(\boldsymbol{k};\boldsymbol{x},t)u_p(\boldsymbol{k}) + W^v(\boldsymbol{k};\boldsymbol{x},t)v_p(\boldsymbol{k}) \quad (8)$$

where $(u_p, v_p) = [u(\boldsymbol{x}_p,t_p), v(\boldsymbol{x}_p,t_p)]$ are the wind modifications at the influence points. It should be kept in mind in the following that although the index p is used for brevity to denote quantities defined at the influence point $\boldsymbol{x}_p, t_p$, these coordinates are, in fact, functions of the coordinates $\boldsymbol{x}, t$ associated with the wave measurement (identified by the index r) and wavenumber $\boldsymbol{k}$. The spectral impact functions W^u and W^v depend on the past evolution of the sea state and form the causal relation between the wind changes at the displaced influence point $(\boldsymbol{x}_p, t_p)$ in the past and the spectral energy changes at the measurement point $(\boldsymbol{x}, t)$.

Small changes d_r in (integral) model data can be linearly related to the perturbation of the local wave spectrum e,

$$d_r = \sum_{\boldsymbol{k}} A_r(\boldsymbol{k})e(\boldsymbol{k}) \quad (9)$$

where the transfer function $A_r(\boldsymbol{k})$ depends on the kind of observed data (i.e., SAR spectrum, significant wave height, etc.). Combining (8) and (9), the modification d_r of some integral model data can then be linearly related to the modification of the velocity components at the set of influence points p which affect the measurement d_r,

$$d_r = \sum_{\boldsymbol{k}} [B_r^u(\boldsymbol{k})u_p(\boldsymbol{k}) + B_r^v(\boldsymbol{k})v_p(\boldsymbol{k})] \quad (10)$$

where

$$B_r^u(\boldsymbol{k}) = A_r(\boldsymbol{k})W^u(\boldsymbol{k}) \quad (11a)$$

$$B_r^v(\boldsymbol{k}) = A_r(\boldsymbol{k})W^v(\boldsymbol{k}) \quad (11b)$$

Substitution of (10) into the cost function (2) yields

$$J = \sum_r [(\sigma_r)^{-2}F_r^2] + H\sum_p [u_p^2 + v_p^2] \quad (12a)$$

where

$$F_r = \Delta D_r + \sum_{\boldsymbol{k}'}[B_r^u(\boldsymbol{k}')u_p(\boldsymbol{k}') + B_r^v(\boldsymbol{k}')v_p(\boldsymbol{k}')] \quad (12b)$$

$\Delta D_r = D_r - D_r^{\mathrm{obs}}$ and $p = p(r,\boldsymbol{k})$. Thus (2) has become a linear optimization problem for the modification in the wind velocity field. From the minimization conditions $\partial J/\partial u_p = 0$ and $\partial J/\partial v_p = 0$ we obtain

$$u_p(\boldsymbol{k}) = -(\sigma_r)^{-2}H^{-1}F_rB_r^u(\boldsymbol{k}) \quad (13a)$$

$$v_p(\boldsymbol{k}) = -(\sigma_r)^{-2}H^{-1}F_rB_r^v(\boldsymbol{k}) \quad (13b)$$

The solution of (13) is given by

$$u_p = K_r\Delta D_rB_r^u \quad (14a)$$

$$v_p = K_r\Delta D_rB_r^v \quad (14b)$$

where

$$K_r = -\left[(\sigma_r)^2H + \sum_{\boldsymbol{k}'}\left\{[B_r^u(\boldsymbol{k}')]^2 + [B_r^v(\boldsymbol{k}')]^2\right\}\right]^{-1} \quad (15)$$

Thus for each spectral wave component $\boldsymbol{k}$ of each measurement r one derives an associated wind correction vector (u_p, v_p) which is proportional to the net spectral impact functions B_r^u, B_r^v of the wave component $\boldsymbol{k}$ and to the difference between the first-guess and the observed wave data ΔD_r. The wind correction vector depends also on the quality of the observations and the integral sensitivity, expressed by the sum in (15).

In the following the main interest will be in the assimilation of measured two-dimensional ocean wave spectra (e.g., SAR or buoy spectral data). In this case a large number of measurements are available for a given position, each spectral measurement at a wavenumber $\boldsymbol{k}$ being regarded formally as a separate data value r. However, from the measurement of a single energy value from only one spectral component it is, in principle, impossible to determine the correction of a two-dimensional wind vector: the deviation between the predicted and observed energy can be due to a change in either the magnitude or the direction of the wind vector at the influence point. The two components of the wind vector can be inferred only if we combine several spectral bins to describe the change in the relative distribution of energy in the spectrum. We shall accordingly consider a cluster of spectral bins $(m \pm s_1, n \pm s_2)$ around a given reference spectral bin (m, n) = (frequency, direction), where $s_1, s_2 = 0, 1$, or 2. For each cluster we introduce three derived data values D_1, D_2, and D_3 representing the mean energy difference and two components of the spectral gradient at (m, n)

$$D_1(m,n) = \frac{1}{2}D(m,n) + \frac{1}{8}[D(m \pm 1, n) + D(m, n \pm 1)] \quad (16)$$

$$D_2(m,n) = \sum_{s=1}^{2}[D(m, n+s) - D(m, n-s)] \quad (17)$$

$$D_3(m,n) = D(m+1, n) - D(m-1, n) \quad (18)$$

We anticipate that changes in the magnitude of the wind will affect mainly the mean energy and the gradient of the spectrum with respect to frequency, while changes in wind direction will modify mainly the derivative of the spectrum with respect to the propagation direction. Tests with various degrees of smoothing in the definition of the mean energy and the derivatives of the spectrum yielded optimal results for the weighting given in (16)–(18).

Thus we rewrite the cost function (12) as

$$J = \sigma^{-2}\sum_{i=1}^{3}(C_i \Delta D_i + d_i)^2 + H\,(u_p^2 + v_p^2) \quad (19)$$

where ΔD_i denote the differences between the first-guess clustered data D_i and observed clustered data D_i^{obs}, d_i is the desired modification of the model first-guess, σ is the rms error of the wave observations, and (u_p, v_p) is the wind correction vector. According to the usual data quality criteria, the error of the wave data observations is set proportional to the wave energy itself. The weights C_i assigned to these different deviations will be adjusted in the calibration process described in section 6.

The three corresponding modifications of the model data are of the general form (see 10)

$$d_i = B_i^u u_p + B_i^v v_p. \quad (20)$$

Substitution of (16)–(18) and (20) into the cost function (19) yields as minimum solution for the wind correction vector (omitting the index p)

$$u = \frac{P_u R_v - P_v R_{uv}}{R_u R_v - (R_{uv})^2} \quad (21)$$

$$v = \frac{P_v R_u - P_u R_{uv}}{R_u R_v - (R_{uv})^2} \quad (22)$$

where

$$R_u = \sigma^2 H + \sum_{i=1}^{3}(B_i^u)^2 \quad (23)$$

$$R_v = \sigma^2 H + \sum_{i=1}^{3}(B_i^v)^2 \quad (24)$$

$$R_{uv} = \sum_{i=1}^{3}(B_i^u B_i^v) \quad (25)$$

$$P_u = -\sum_{i=1}^{3} C_i \Delta D_i B_i^u \quad (26)$$

$$P_v = -\sum_{i=1}^{3} C_i \Delta D_i B_i^v. \quad (27)$$

The outputs of the wave data assimilation scheme are wind vector modifications which are distributed in space and time in accordance with their effective impact on the wave spectra at the various measurement points. Each measured spectrum produces a large number of wind vectors. The introduction of clustered spectral data in place of the original spectral values does not yet lead to a reduction of this number, since the central bin (m, n) of a cluster runs through all spectral bins for those where the cluster lies within the definition domain of the spectrum. However, one should clearly not regard single spectral wave measurements as independent measurements but as coherent ensembles. Thus one needs to gather and appropriately average all wind correction vectors which belong to a common influence region. In general, this represents a data assimilation task in which the wind corrections derived from the wave data should be combined with first-guess information from an atmospheric model forecast and conventional meteorological data to reconstruct an optimum, dynamically consistent wind field. This is beyond the scope of the present paper, however, and we shall apply a simpler averaging method.

Once the wind field has been corrected, the wave field can be recomputed using the modified wind field to drive the wave model. Should the wave corrections computed from the wind corrections, as inferred from the linearized wave model, turn out to be inadequate, the recomputed "second-guess" wave data can be used as a starting point for a second wave data assimilation cycle. If necessary, the iteration can be repeated several times. In this manner one can, in principle, overcome the limitations of the linearization (in the same way as in the adjoint technique, although there, several itera-

tions are always necessary to find the cost minimum, which in our method is computed explicitly). However, since our method involves other unavoidable approximations in the computation of the impulse response function of the wave model, in most cases the approximations incurred by the linearization will be acceptable.

4. The δ-Function Approximation of the Wind Impact Function

To justify the δ-function approximation of the impact functions $W^u(\boldsymbol{k})$ and $W^v(\boldsymbol{k})$ appearing in (7) and to determine the region of maximum impact (i.e., the wave age), we need to investigate now the properties of the functional derivative $\Lambda = \delta S_t/\delta E$ and the derivative $\partial S_t/\partial \boldsymbol{U}$ in (4). The total source function in (3) generally consists of the sum of the input, nonlinear transfer, and dissipation source functions

$$S_t = S_{in} + S_{nl} + S_{ds}. \tag{28}$$

The exact form of the matrix Λ is rather complicated, since S_{ds} and, in particular, S_{nl} are complex nonlinear functions of E. In the implicit integration scheme of the WAM model an approximation of Λ is used in which only the diagonal part of the operator is retained. In this case the operator is reduced to the form $\Lambda = \lambda I$, where I is the identity matrix and λ is a scalar feedback coefficient. We shall use this approximation in the following, with a modification discussed below.

In the source functions of the WAM model the dependence on the wind velocity $\boldsymbol{U}$ appears explicitly only in the input source function S_{in}, which is proportional to the spectrum, so that

$$\frac{\partial S_{in}}{\partial \boldsymbol{U}} = \boldsymbol{a} k E \tag{29}$$

where the vector $\boldsymbol{a}$ is a nondimensional function of $\boldsymbol{U}$. This yields a linearized wave transport equation of the form

$$\left(\frac{D}{Dt} - \lambda\right) e = \boldsymbol{a} \cdot \boldsymbol{u} k E. \tag{30}$$

The limitation to a diagonal feedback term, however, has some basic physical shortcomings. Although not serious when used in the implicit integration scheme of the model, these lead to unrealistic results in the present application. The nondiagonal elements in the functional derivative of S_{nl} result from the nonlinear coupling combinations which are responsible for the transfer of energy across the spectrum. If only the diagonal elements are retained, a perturbation of the spectrum e at a given wavenumber induced by a perturbation of the wind $\boldsymbol{u}$ (which is proportional to the unperturbed spectrum E; see (30)) simply relaxes back exponentially at a rate governed by the (generally negative) feedback factor λ, without changing other regions of the spectrum.

In reality, however, a perturbation in the wind forcing induces an energy transfer between the various interacting spectral quadruplets in a process which maintains a quasi-similar shape of the spectrum. Small perturbations in the spectrum disappear rapidly through this shape-stabilizing effect of the nonlinear transfer S_{nl}, while at the same time the peak of the spectrum (for positive wind perturbations) is shifted to lower frequencies [*Hasselmann et al.*, 1973]. Numerical experiments by *Hasselmann and Hasselmann* [1985], *Resio and Perrie* [1991], and *Young and Van Vledder* [1993] have demonstrated that negative and positive energy perturbations at frequencies larger than the peak frequency are quickly compensated by an energy flux from and to neighboring spectral components, respectively, to recover an approximate f^{-4} distribution corresponding to the constant-flux cascade [*Zakharov and Filonenko*, 1967]. A change of only the wind direction causes positive and negative energy changes which are largest for the propagation directions whose spectral spreading function is changing most rapidly. The resulting rotation of the spectrum is again controlled largely by S_{nl} [*Young et al.*, 1987; *Young and Van Vledder*, 1993].

To account for these nondiagonal energy transfers, we replace the source function appearing on the right-hand side of (30) by an effective driving source function which is expressed as a linear combination of the source functions S_{in} and S_{nl}. Experiments with a number of different forms yield optimal results for the following parameterization. For a wind perturbation u' parallel to the first-guess wind $\boldsymbol{U}$ we describe the evolution of the spectral perturbation by

$$\left(\frac{D}{Dt} - \lambda\right) e^{\parallel} = \beta'_u u' \tag{31}$$

where

$$\beta'_u = \begin{cases} a_1 \frac{k}{\omega}(0.5 S_{in} + S_{nl}) \cos(2\vartheta) & |\vartheta| \le \pi/4 \\ 0 & |\vartheta| > \pi/4. \end{cases} \tag{32}$$

$\vartheta = (\theta - \theta_w)$ where θ and θ_w are the directions of the wave component and of the local wind, respectively. Thus a change of the wind speed is assumed to cause a maximum energy change for wave components propagating in the direction of the wind, the energy changes decreasing to zero at $\pm 45°$ from the wind direction.

For a wind perturbation v' orthogonal to the first-guess wind direction we assume the solution

$$\left(\frac{D}{Dt} - \lambda\right) e^{\perp} = \beta'_v v' \tag{33}$$

where

$$\beta'_v = \begin{cases} a_2 \frac{k}{\omega} \frac{\partial}{\partial \theta}(S_{in} + 0.5 S_{nl}) |\sin(2\vartheta)| & |\vartheta| \le \pi/4 \\ 0 & |\vartheta| > \pi/4. \end{cases} \tag{34}$$

The directional gradient produces an antisymmetric pattern. The pattern has extreme values in the neighborhood of $\pm 45°$ from the spectral peak. The values of the free coefficients a_1 and a_2 were estimated by the calibration process described in section 6.

For unit wind field perturbations in the x and the y directions, evolution equations were inferred for the

spectral impact functions W^u and W^v, respectively

$$\left(\frac{D}{Dt} - \lambda\right) W^{u,v} = \beta_{u,v} \tag{35}$$

where

$$\beta_u = \beta'_u \sin\theta_w - \beta'_v \cos\theta_w \tag{36}$$

$$\beta_v = \beta'_u \cos\theta_w + \beta'_v \sin\theta_w. \tag{37}$$

The source functions in (35) are obtained by transforming the source functions in (31) and (33) from the (u', v') system oriented with respect to the local wind direction into the standard (u, v) system of the WAM model in which the wind direction θ_w and the wave propagation direction θ are defined clockwise from north.

Equations (31) and (33) describing the linear response of the wave spectrum to perturbations in the wind field do not yet contain the δ-function approximation. This we deduce now from the properties of the damping factor λ and the wind impact factors $\beta_{u,v}$ in (35). Consider the application of a uniform wind field perturbation to a nonuniform background wind field, with an accompanying background wave field consisting of the usual admixture of wind sea and swell. The combination of the forcing and damping terms in (31) and (33) have the effect that for each energy-containing spectral component there is only a limited region of the perturbed wind field which has a significant influence on the spectral response. This is the region in which the wave component last experienced a significant forcing from the effective driving source functions expressed in (32) and (34). Before this last forcing, the impact of the wind field perturbation is largely lost through the nonlinear interactions which continuously restore the balance with the rest of the spectrum. This is associated with a large nonlinear damping factor λ. Once the wind sea has been converted to swell, the exponential damping vanishes, but the driving source function is then also zero.

Hence the most effective region for modifying the spectral swell energy is the narrow transition area between wind sea and swell. This region of effective wind impact can be determined from the wave age $\tau_p(\boldsymbol{k})$, the time of travel from the impact region to the measurement point. If the wave component is a wind sea component, rather than swell, the most sensitive region is close to, but upwind from, the measurement point, the effective distance upwind depending on the fetch or duration and the wind speed.

To specify the different regions of origin for the spectral wave components, we compute the spectral wave age $\tau_p(\boldsymbol{k})$ in a manner similar to the method of *Booij and Holthuijsen* [1987]. From the time t and the position $\boldsymbol{x}$ of the spectral measurement each wave component can be traced back along its great circle path to its effective point of origin $(\boldsymbol{x}_p, t_p)$, where (in simplified Cartesian notation)

$$t_p(\boldsymbol{k}) = t - \tau_p(\boldsymbol{k}) \tag{38}$$

$$\boldsymbol{x}_p(\boldsymbol{k}) = \boldsymbol{x} - \tau_p(\boldsymbol{k})\boldsymbol{c}_g \tag{39}$$

and $\boldsymbol{c}_g$ is the group velocity.

Booij and Holthuijsen [1987] defined the time of origin t_p of a wave component $\boldsymbol{k}$ as the average time weighted with the integrated "active source function" for that component. For our application we define t_p as a weighted average time through the relation

$$t_p(\boldsymbol{k}) = T^*/W^* \tag{40}$$

where T^*, W^* are determined by integrating the propagation equations

$$\left(\frac{D}{Dt} - \lambda\right) T^*(\boldsymbol{k}; \boldsymbol{x}, t) = \beta t \tag{41}$$

$$\left(\frac{D}{Dt} - \lambda\right) W^*(\boldsymbol{k}; \boldsymbol{x}, t) = \beta \tag{42}$$

where β denotes the modulus $\beta = ({\beta'_u}^2 + {\beta'_v}^2)^{1/2}$ of the wind impact coefficients β'_u, β'_v in (31) and (33). Equation (41) clearly has the desired property of weighting those time periods for which β is large and the damping λ small. The second equation, (42), supplies the normalizing factor W^* for this calculation.

In summary, in order to derive the influence point $(\boldsymbol{x}_p, t_p)$ and the wind impact functions W^u, W^v, we need to integrate the four propagation equations for the spectral variables T^*, W^*, W^u, and W^v. This can be done efficiently in the course of the basic wave model integration. Since no additional source functions need to be computed and, in the case of the WAM model, the propagation computation is less time-consuming than the evaluation of the total source function, the computational overhead remains acceptable. However, the storage requirements are increased by a factor of approximately 4.

5. Numerical Implementation

As in the numerical scheme of the WAM model, the propagation for the additional impact variables T^*, W^*, W^u, and W^v is performed by an upwind-flux scheme. However, instead of the implicit integration method used to integrate the full source function S_t in the WAM model, an alternative, more efficient analytical technique is applied which makes use of the property that the additional transport equations are linear in the impact variables.

The integration of one forcing time step for the impact variables requires the integration of an equation of the form

$$\frac{dy}{dt} = \alpha + \lambda y. \tag{43}$$

As both α and λ can be regarded as constant over the integration time step Δt, a local analytical solution of (43) can be found [*Sobey and Young*, 1986]

$$y^{n+1} = y^n e^{\lambda\Delta t} + \frac{\alpha}{\lambda}\left[e^{\lambda\Delta t} - 1\right] \tag{44}$$

where n and $n+1$ refer to the time level of the solution, $\alpha = \alpha^n$ and $\lambda = \lambda^n$. For the case of no damping, i.e., $\lambda = 0$, a series expansion of the exponential function in

(44) yields the expected result of an unlimited growth

$$y^{n+1} = y^n + \alpha \Delta t. \tag{45}$$

Tests have shown that this scheme maintains numerical stability at the source function time step of the WAM model (which is an order of magnitude larger than the time step required for an explicit scheme).

As mentioned earlier, the feedback λ is strongly negative in the wind sea portion of the spectrum. However, in some regions, normally close to the high-frequency side of the spectral peak, λ may become slightly positive. Since λ is intended to act as a damping term, the positive feedback is suppressed by setting λ equal to zero in these regions.

We note that the form of the forcing terms (32) and (34) was chosen to capture both the wind input forcing and the energy transfer between spectral components which appear in the nondiagonal elements of the source term derivative Λ. Since the form should relate directly to the local wind, spectral regions of the source terms which are not closely coupled to the local wind have been excluded by setting $\beta_u, \beta_v = 0$ for $f < 0.8 f_{\mathrm{PM}}$ or $|\theta_w - \theta| > \pi/2$, where f_{PM} is the Pierson-Moskowitz frequency and θ, θ_w denote the wave propagation and wind direction, respectively. The calculations are performed using the standard WAM model cycle 4, with 25 logarithmically spaced frequencies f_n of resolution $\Delta f_n / f_n = 0.1$ and a directional resolution of 15°.

6. Calibration of the Assimilation System

The forms (32) and (34) for the wind impact factors β'_u, β'_v in the perturbation equations (31) and (33), respectively, were tuned to reproduce as closely as possible the spectral perturbations induced by small wind field changes for the simplest geometry of fetch-limited wave growth. The properties of the wind impact functions are shown for a fully developed (600-km fetch, 5.5-day integration time) reference spectrum in Figure 1. This spectrum is generated by a homogeneous, stationary, northward blowing, 10-m wind $(U, V) = (0{,}10\ \mathrm{m/s})$, yielding a significant wave height of 2.10 m.

The pattern of the impact function $W^v(\boldsymbol{k})$ corresponding to wind changes in the y direction (Figure 2a) compares well with the energy differences between a perturbed and the reference spectrum computed with the WAM model (Figure 2b). The perturbed spectrum was obtained by adding a homogeneous wind field change of $(u, v) = (0{,}1\ \mathrm{m/s})$, i.e., by increasing the wind speed by 10%. This leads to an increase in the wave height of about 20% (0.5 m).

The second impact function $W^u(\boldsymbol{k})$ corresponding to wind changes in the x direction is shown in Figure 3a, and the corresponding change in the spectrum for a 10% wind perturbation orthogonal to the initial wind is presented in Figure 3b. The perturbation yields a spectrum rotated by about 6°, with essentially no change in total energy. The computed spectral differences between the rotated and the reference spectrum exhibit a plus–minus pattern centered at ±45° off the initial spectral peak, which is similar to the distribution of W^u.

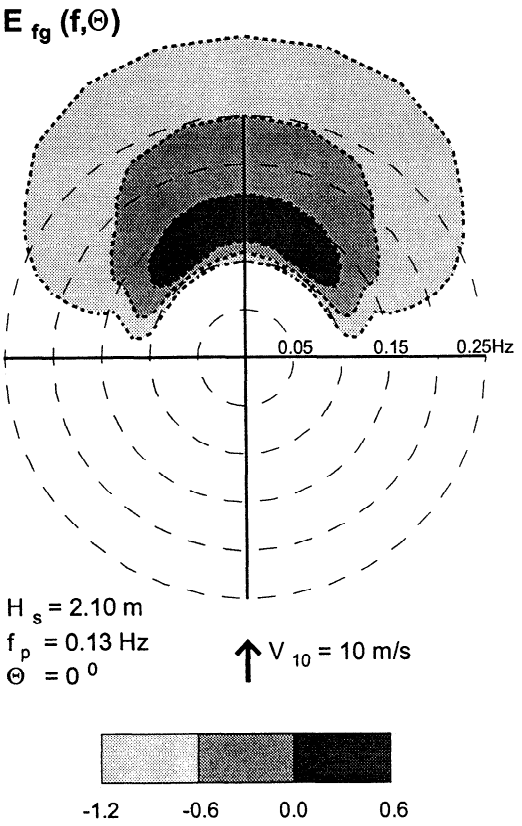

Figure 1. Polar plot of fetch-limited (essentially fully developed) first-guess spectrum $E(f, \theta)$ at 6°N, 23°E generated by a homogeneous, stationary wind field with (U, V)=(0,10) m/s and an upwind boundary at the equator. The significant wave height is 2.10 m, the peak frequency is 0.13 Hz, and the peak direction is 0°. Isolines of the spectral energy are scaled logarithmically. Dashed circles are frequency isolines in steps of 0.05 Hz.

In agreement with the energy changes derived directly from the WAM model, the sensitivity of the wind impact functions W^u and W^v is largest for frequencies in the vicinity of the peak frequency and falls off rapidly toward higher frequencies. The high-frequency falloff, due to the exponential decay factor λ in (31) and (33), does not imply that the higher-frequency components do not respond to a perturbation of the wind but, rather, that the response information is lost due to the rapid readjustment of the spectrum toward a quasi-universal form.

Despite the overall agreement of the distribution of the spectral changes computed by the Green's function method and directly by the WAM model, the ratios of the impact functions W^u and W^v and the corresponding energy differences from the WAM model calculations, respectively, are not constant (Figures 2c and 3c). Thus wind field corrections computed by the Green's function method from different components of the spectrum vary. To overcome such variations, the spectral wind corrections corresponding to a given region of in-

fluence are collected into clusters to form appropriately weighted mean wind correction vectors.

Various methods can be devised to collect and average the wind correction vectors associated with a common region of influence. The most satisfactory technique is presumably to base the clustering criterion on the wave ages and the resulting locations and times of origin $(\boldsymbol{x}_p, t_p)$ of each spectral component. However, here a simpler method is used which enables the present wave data assimilation scheme to be related to an alternative wave data assimilation method which corrects only the local wind. The latter method, designed for the assimilation of SAR-retrieved wave spectral data, is currently in a preoperational testing phase at the European Centre for Medium-Range Weather Forecasts (ECMWF). The method is based on an extension of the current ECMWF operational optimum interpolation method for assimilating ERS-1 radar altimeter data in the WAM model and involves a decomposition of the wave spectrum into principal wave systems $E_j(f,\theta)$, with $E(f,\theta)=\sum_j E_j(f,\theta)$ using a modified form of *Gerling's* [1992] partitioning method [*Brüning et al.*, 1994]. The wave systems $E_j(f,\theta)$ are assigned to a separate, nonoverlapping region Ω_j of the (f,θ) plane in accordance with a simple "inverted catchment area" algorithm.

We use this partioning scheme to define an average wind field correction (u_j, v_j) for a given wave system E_j through

$$\begin{pmatrix} u_j \\ v_j \end{pmatrix} = \frac{\int_{\Omega_j} \begin{pmatrix} u(f,\theta) \\ v(f,\theta) \end{pmatrix} E_j(f,\theta) df d\theta}{\int_{\Omega_j} \begin{pmatrix} M_u(f,\theta) \\ M_v(f,\theta) \end{pmatrix} E_j(f,\theta) df d\theta} \tag{46}$$

where $u(f,\theta), v(f,\theta)$ denote the wind field correction for each frequency-direction bin of the wave system E_j. A masking factor

$$M_{u,v}(f,\theta) = \begin{cases} 0 & : \; u(f,\theta), v(f,\theta) = 0 \\ 1 & : \; u(f,\theta), v(f,\theta) \neq 0 \end{cases} \tag{47}$$

has been introduced to filter out spectral components in the normalizing integrals those wind field corrections vanish. (The impact factors W^u, W^v are set to zero when they fall below a model noise limit of 1% of the maximum value of W^u or W^v for the given spectrum.) The effective location $(\boldsymbol{x}_j, t_j)$ of the mean wind field correction for a given wave system E_j is computed from the mean wave age τ_j, mean frequency f_j, and mean direction θ_j (defined as $\tan^{-1}[(\sin\theta)_j/(\cos\theta)_j]$), where

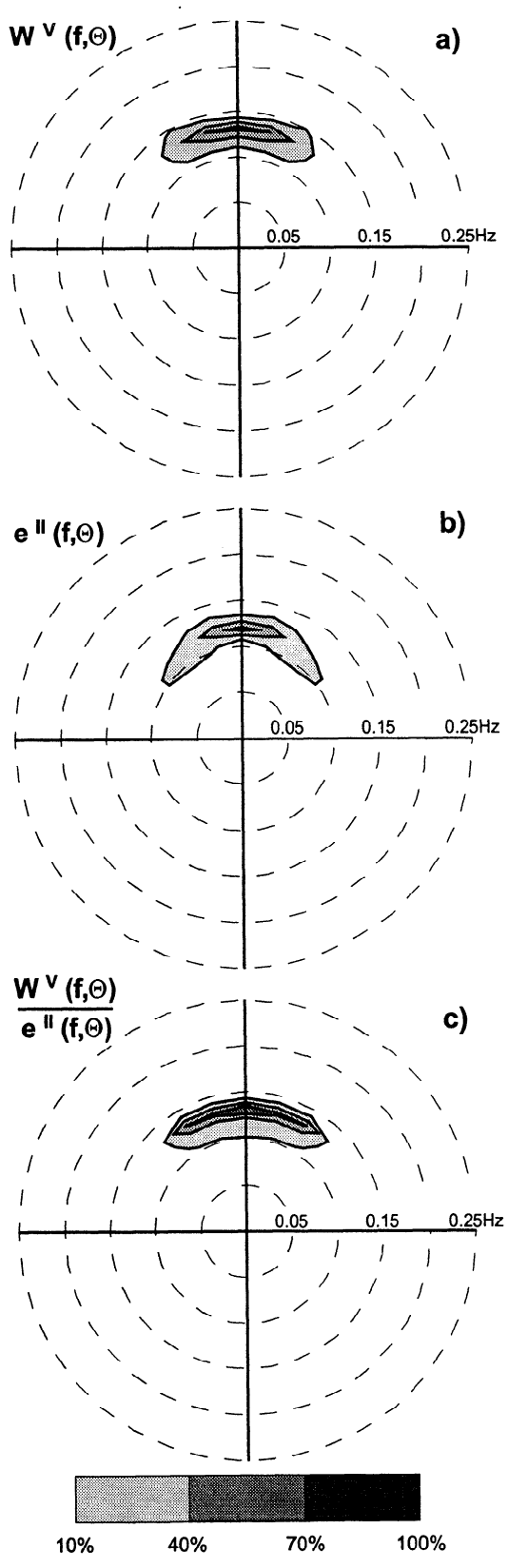

Figure 2. (a) Wind impact function $W^v(f,\theta)$ for the first-guess spectrum of Figure 1, showing the response of the spectrum to a unit change of the wind in the y direction. (b) Difference $e(f,\theta)$ between a perturbed spectrum generated by a homogeneous wind field with (U,V)=(0,11) m/s and the first-guess spectrum of Figure 1 with (U,V)=(0,10) m/s. The difference in significant wave height is 0.48 m. (c) Ratio between the wind impact function W^v and the computed spectral perturbation e. Isolines represent the percentage of the maximum of each distribution in 30% intervals.

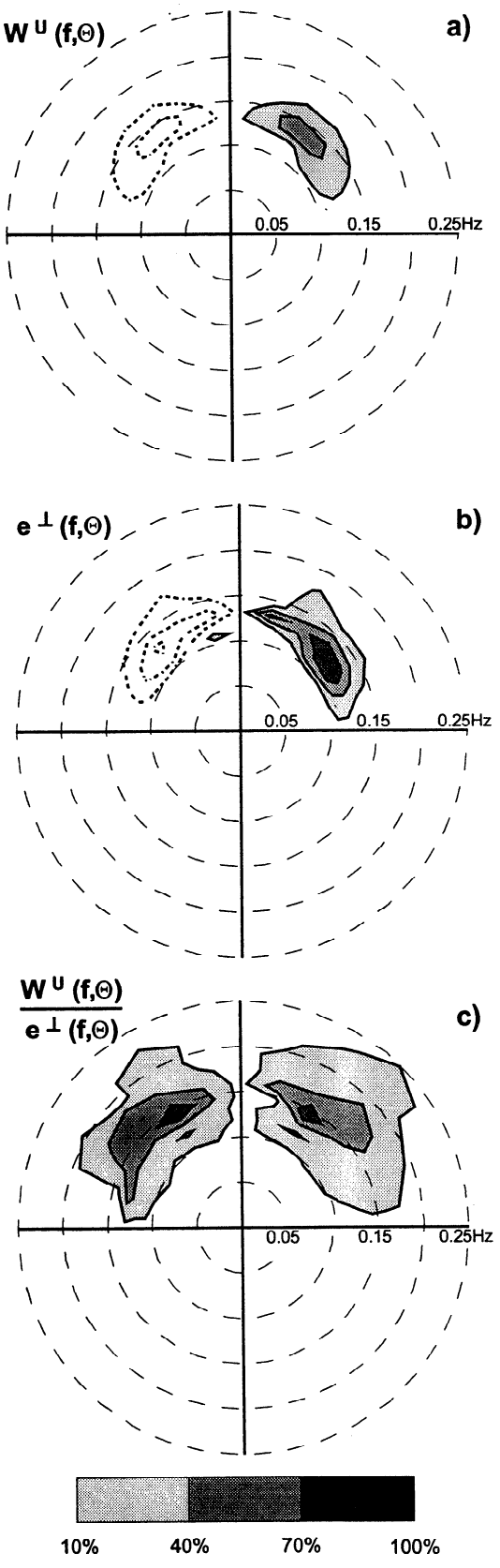

Figure 3. Same as Figure 2, but for the wind input function $W^u(f,\theta)$ and a wind field (U,V)=(1,10) m/s perturbed in the cross-wind direction x. The difference in significant wave height for the reference and perturbed runs is 0.02 m. Shaded areas represent positive values, dotted isolines correspond to negative values.

$(\sin\theta)_j, (\cos\theta)_j$ are averages defined in accordance with (46)) using the relations (38) and (39).

To calibrate the procedure, the magnitudes of the computed wind changes were adjusted through a suitable choice of the free scaling coefficients a_1, a_2, and $C_i (i = 1, 3)$ in (32), (34), and (19). The calibration was performed for the case of an almost fully developed, fetch-limited (500-km fetch, 5.5-day duration) reference "first-guess" spectrum generated by a homogeneous wind field with (U, V) = (0,14 m/s). The wind field was then perturbed by 10% in the x and the y directions to produce two so-called "observed" spectra. The wind field errors were then inferred from the assimilation of the observed spectra. The five coefficients of the wind correction algorithm were determined simultaneously by minimizing the sum, from both assimilation cases, of the differences between the prescribed errors in the first-guess wind field and the wind correction vectors inferred from the assimilation algorithm. Precalculated first estimates of the coefficients were used as starting values for the minimization procedure using an unconstrained conjugate gradient scheme. To obtain a stable solution it was found advantageous to smooth the effective driving functions in (32) and (34) by a three-point running mean. The optimal scaling coefficients for the wind impact functions (32) and (34) were found to be $a_1 = 33.6, a_2 = 8.2$, while the optimal weights in the cost function (19) were $C_1 = 9.92, C_2 = 4.66$, and $C_3 = 0.1$. The weight of the side condition penalizing excessively large wind corrections was set as $II = 10$.

7. Verification of the Wind Field Corrections

In the following the performance of the calibrated Green's function assimilation scheme is tested under three different sea state conditions. To yield a controlled experiment, synthetic, rather than true, observed data were used. For each test case the WAM model was run twice, once for the reference wind, yielding the first-guess wave spectrum, and once for a perturbed wind field, yielding the observed spectrum. The test area was taken again as the 40×25 longitude, latitude rectangular box, with a resolution of 1° × 1° and the equator as the southern boundary.

The first sea state condition represents a generalization of the fetch-limited, fixed-fetch case which was used to calibrate the assimilation scheme. The first-guess wave spectrum was computed, as in the calibration case, for a homogeneous, northward directed wind field, but the wind speed was now taken as 18.45 m/s instead of 14 m/s. The wind was then changed by 10% in the y and the x directions to produce two sets of observed spectra. From the assimilation of these observed spectra, mean wind correction vectors directed to the north and east, respectively, were obtained. The magnitudes of the wind corrections are presented as a function of latitude (corresponding to nondimensional fetch values gx/U^2 between about 2.5×10^3 and 6×10^4) in Figures 4a and 4b, respectively. Both prescribed wind field per-

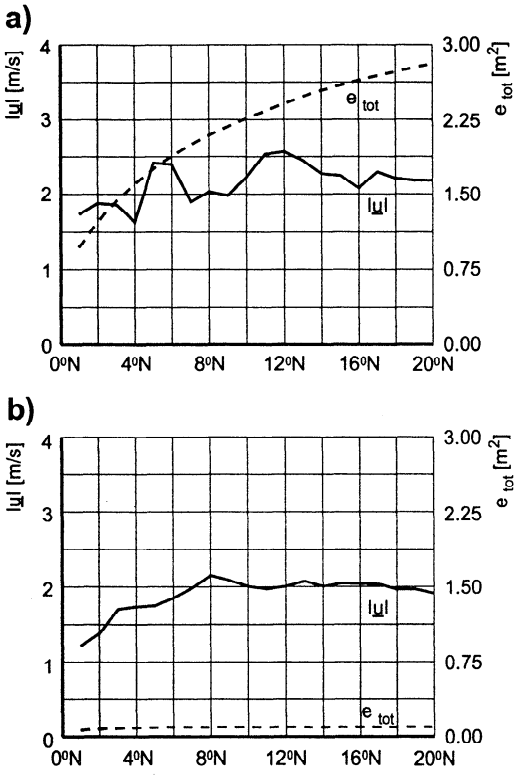

Figure 4. Computed wind corrections for the fetch-limited case with 18.45 m/s winds blowing northward. (a) Homogeneous wind speed change of 10% in y (northward) direction. (b) Homogeneous wind speed change of 10% in x (eastward) direction. In Figure 4a the computed wind corrections (solid line) fluctuate weakly about the prescribed wind change of 1.85 m/s, the differences in total energy between the perturbed and the first-guess spectra (dashed line) increasing, as expected, with fetch. In Figure 4b the computed wind corrections (solid line) are also close to the prescribed wind change, while the differences in total energy (dashed line) are negligible.

turbations, causing an increase and a rotation of the spectra, respectively, could be retrieved reasonably accurately, with some variation about the expected mean value of 1.85 m/s. As predicted theoretically, the differences in total energy between the first-guess spectra (U = 18.45 m/s) and the spectra with enhanced wind speeds (U = 20.3 m/s) increase with fetch (Figure 4a), while the change in the wind direction causes no significant change in energy (Figure 4b). As a test of the nondimensional fetch scaling laws, the experiment was repeated using winds of 14 and 10 m/s instead of 18.45 m/s, with essentially the same results.

The second synthetic sea state condition was devised to test the applicability of Green's function assimilation scheme for swell, where the magnitude, direction, and location of the wind correction vector are far from the measurement location. The same grid was used as before, with a uniform wind of (U, V)=(0,10 m/s) blowing northward. However, now a small region, 17°N – 19°N, 28°E – 29°E, of intense winds, represented by six grid points, was introduced in the northeast of the experimental area. The wind velocity was set to 30 and 33 m/s in the direction of 220° for the first-guess and observed data runs, respectively. The first-guess wind field and the resulting wave heights in the central part of the grid are shown in Figures 5a and 5b, respectively. The

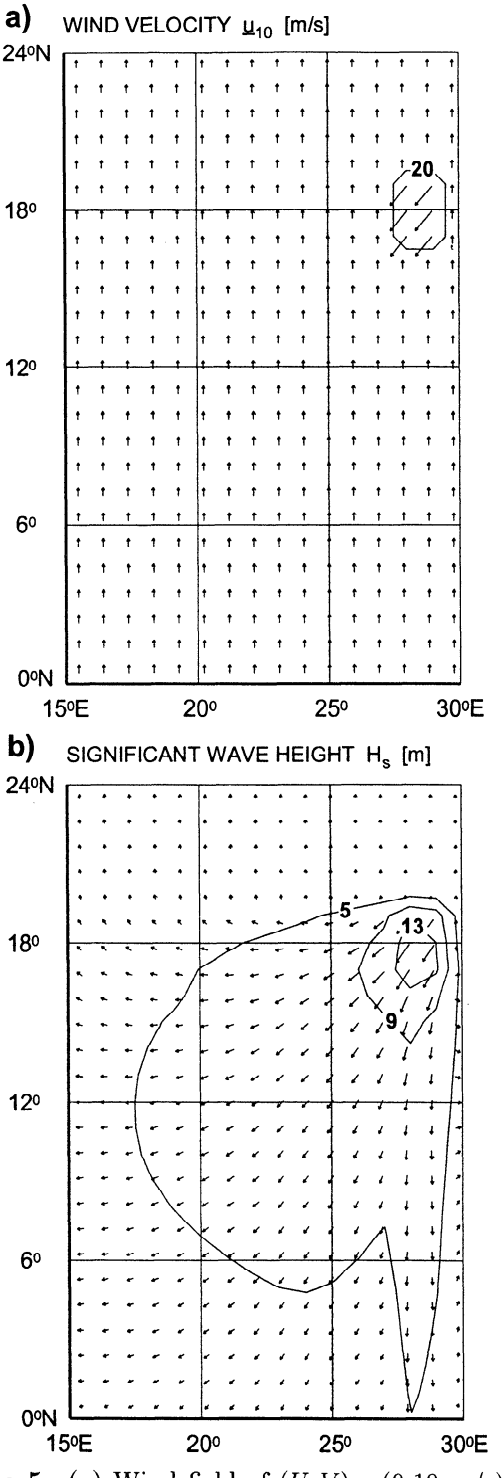

Figure 5. (a) Wind field of (U, V) =(0,10 m/s) with an inset region of strong winds with (U, V) = (30 m/s, 220°) in the northeast of the model area that produced (b) a wave field. The waves consist of wind sea and swell, attaining a maximum significant wave height of more than 13 m.

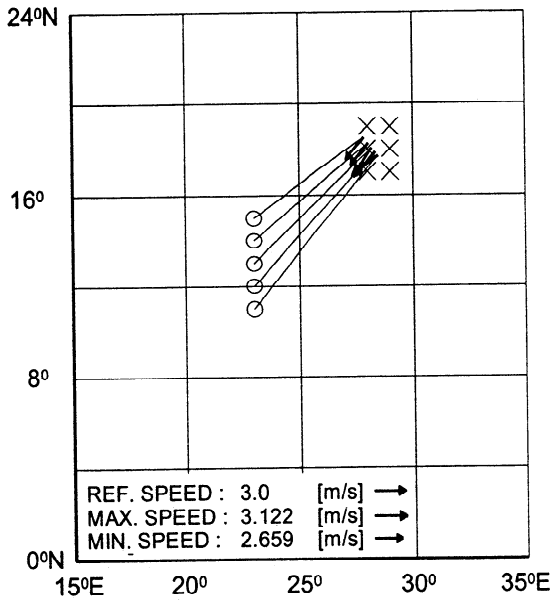

Figure 6. Mean wind correction vectors for the case shown in Figure 5 obtained by the assimilation of five observed spectra located at positions marked by circles. The observed spectra differ from the first-guess spectra through a stronger swell. This was generated by a 10% increase in the wind from 30 m/s, 220° to 33 m/s, 220° at the positions marked by crosses. All five wind correction vectors reproduce the prescribed wind change of approximately 3 m/s, 220° at the correct location (lines connecting the circles and crosses indicate the great circle propagation paths of the swell).

waves leaving this strong local wind field propagated into the rest of the region as swell. As the swell generation region approximates a spatial δ-function, this configuration provides a useful test for validating the computation of the spectral wave age needed to locate the swell source region. In addition, it tests the magnitude and direction of the computed wind vector corrections under conditions which differ significantly from the fetch-limited case used to calibrate the wind correction algorithm.

The mean wind correction vectors were inferred from wave measurements downwind of the swell source region at 11°N – 15°N along 23°E. The values lie close to the expected value of (3 m/s, 220°) (Figure 6). The locations of the wind correction vectors were computed from the mean wave age τ_j of the swell, which was represented as a partitioned wave system with mean frequency f_j, mean direction θ_j, and mean group velocity c_{gj}. Tracing back from the observation point along the great circle path of the swell, the computed wave age yields exactly the swell source region as the location of the wind correction (Figure 6). No corrections of the wind field are obtained outside the swell source region, since no differences are found between model and observed data for the wind sea wave components. In a complementary experiment in which observed and first-guess spectra were interchanged, the wind speed reduction could also be retrieved and located correctly. (To exclude wave ages computed for spectral components with very little energy, which are contaminated by numerical model noise, all wave ages for which W^* is less than 1% of the maximum value of W^* for the given spectrum were again excluded.)

In a third test case the focus was placed on the retrieval of the wind corrections from more complex spectra consisting of a superposition of wind sea and swell with different propagation directions. The first-guess wave field was generated by relatively strong cyclonic winds representing an idealized atmospheric low-pressure system. The cyclonic wind system of about 18.3 m/s was embedded in the center of the experimen-

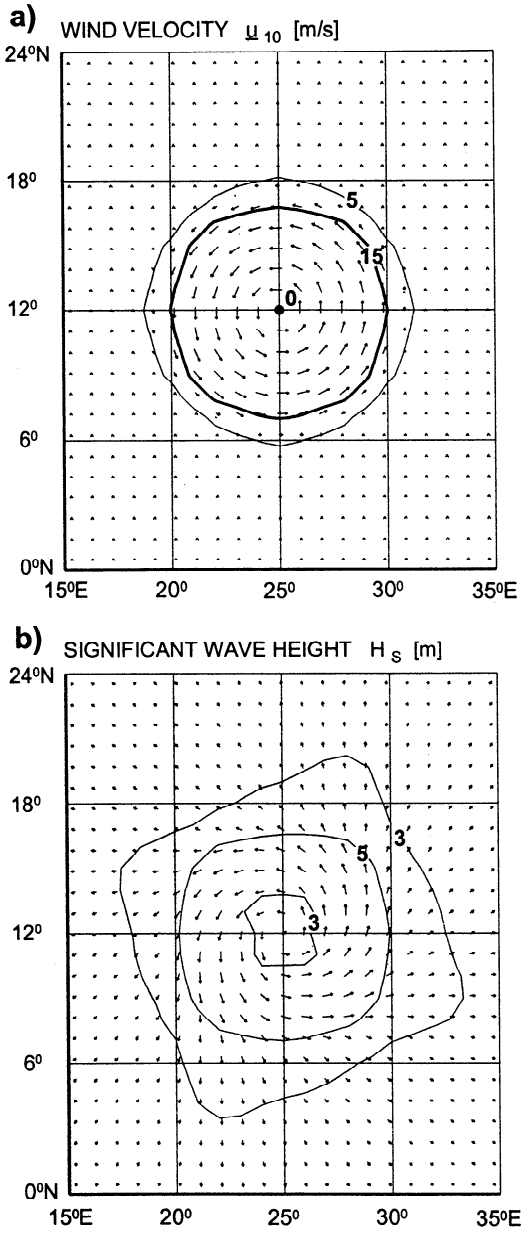

Figure 7. (a) Cyclone with wind speeds of $|U|$=18.3 m/s embedded in a northward wind of 2 m/s producing a (b) wave field. The cyclonally traveling waves attain significant wave heights of the order of 6 m and propagate out of the generation region into the model area as swell.

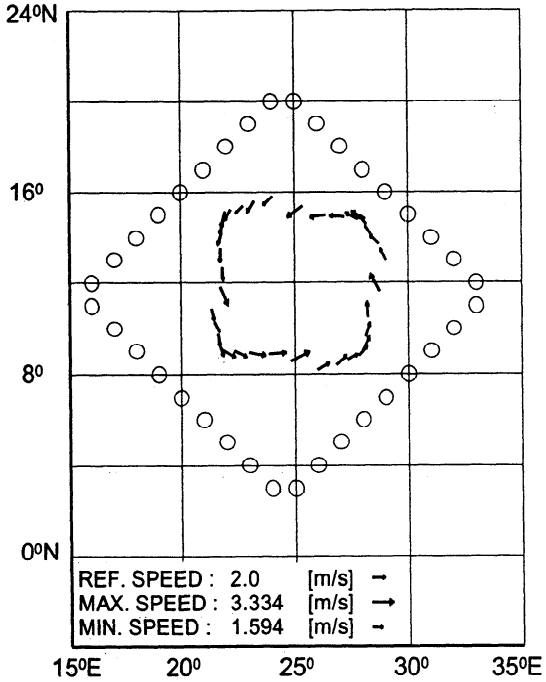

Figure 8. Mean wind correction vectors derived from the assimilation of 36 observed spectra at locations (circles) corresponding to typical ERS-1 and ERS-2 synthetic aperture radar wave mode sampling. The observed spectra are generated by a cyclone with winds which are increased by 10% relative to the first-guess cyclone in Figure 7a. Most of the spectral energy deviations represent swell observed outside the generation region. The magnitudes of the computed wind correction vectors are about 2 m/s, while the directions reproduce the circular storm pattern, in general agreement with the prescribed errors of the first-guess cyclonic wind field.

tal area with a very weak northward blowing homogeneous wind field of 2 m/s (Figure 7a). The maximum significant wave heights are approximately 6 m (Figure 7b).

The observed spectra were computed by increasing the cyclonic wind field by 10%. The locations of the observation were chosen in accordance with the geometry of the wave spectral data which could be retrieved from the SAR wave mode of the European Remote Sensing Satellites ERS-1 and ERS-2. The locations were spaced about 200 km apart along descending and ascending orbits which were assumed to bracket the cyclonic wind system. From the assimilation of these observed spectra the errors in the swell components of the spectra were clearly shown to originate from the cyclone and to be caused by an underestimation of the cyclonic wind by about 2 m/s (Figure 8). However, four of the wind corrections are seen to be overpredicted by about 50%. They originate from either 12° latitude or 25° longitude, where several wind vectors are aligned with spectral direction bins (note the corresponding distortion of the isolines of the significant wave heights in Figure 7b). This suggests that the overestimated wind correction can be partly attributed to the garden sprinkler effect of the numerical propagation scheme. In time-varying situations this effect will presumably be negligible. Similar analyses for a 14 m/s cyclonic wind system or with an increase in the strength of the background wind field from 2 to 5 m/s yielded essentially the same results. The results of these tests clearly demonstrate that it is possible to deduce both the wind correction vectors and the locations and times of the wind corrections from spectral energy measurements at distant locations and later times.

8. Conclusions

The Green's function assimilation method presented here represents the first step toward a comprehensive data assimilation system for atmospheric and wave data using both atmospheric and wind wave models, ideally in a coupled mode. The technique uses observed wave data to derive corrected wind fields which are dynamically consistent, in an optimal least square sense, with the WAM wave model. The corrected wind data can then be used to recompute a corrected wave field (although this subsequent step was not performed in the present paper).

The method should prove particularly useful in extreme wind situations, which are often inadequately resolved or missed in operational forecasts. This is important mainly for the Southern Ocean, where data coverage is sparse; but severe events can also be poorly captured in the northern hemisphere. A specific case was Hurricane Andrew, which occurred in the tropical Atlantic in August 1992 and produced serious damage in eastern North America. The storm was not adequately resolved in the model predictions, although it was clearly visible in Meteosat images. The assimilation of remote-sensed wave data with the present scheme should lead to improved wind analyses and forecasts in such situations.

In addition to forecasting and hindcasting applications, wave data assimilation provides an important tool for investigating the dynamics and improving the modeling of the coupled atmosphere-wave-ocean system. Continuous observations of waves from satellites such as ERS-1 and ERS-2 with altimeters and SARs provide information both on the locally generated wind waves and on swell generated by distant wind systems. While the assimilation of altimeter wave height data requires rather ad hoc assumptions regarding the distribution of the measured total wave energy over the wave spectrum, SAR image spectra yield information on the full two-dimensional wave spectrum. The Green's function assimilation method presented here is particularly useful for the assimilation of two-dimensional wave spectra retrieved from SAR image spectra [*Hasselmann and Hasselmann,* 1991; *Brüning et al.,* 1994; *Bauer,* 1994]. It enables the systematic study of the interrelationship between global wind and wave fields.

The partitioning of the wave spectrum into separate wave systems, together with the computation of the

wave ages defining the location and time of the maximum impact of the wind on the individual wave systems, yields separate wind corrections for each of the wave systems emanating from different generation regions. Combined with analyses of the change in energy of the wave systems as they propagate over large distances in the oceans, the Green's function assimilation method therefore should provide an important tool for distinguishing between wind field errors and model errors in comparisons between predicted and observed wave spectra.

The computation of the impulse response function by inversion of the linearized wave model equations was feasible only through the introduction of several approximations. Foremost among these was the assumption that the region of wind impact can be approximated by a δ-function. Although only physically, rather than mathematically justified, the assumptions were validated in a number of tests with synthetic wind fields. The locations, times, magnitudes, and directions of prescribed wind field errors could be recovered for a variety of wind fields of different geometry. The robustness of the Green's function technique has been demonstrated also in an analysis of ERS-1 SAR wave mode data in the Atlantic [*Bauer,* 1994] and will be further tested in ongoing studies using ERS-1 and ERS-2 data.

Acknowledgments. This study is funded within the research program "Klimarelevante Prozesse im System Ozean–Atmosphäre–Kryosphäre" (SFB 318) of the Deutsche Forschungsgemeinschaft, and contributes to the Pilot-Project PP2-D1 "Derivation and assimilation of ERS-1 wind and wave data."

References

Bauer, E., Assimilation of ocean wave spectra retrieved from ERS-1 SAR into the wave model WAM, in *Proceedings of the Second ERS-1 Symposium: Space at the Service of our Environment, Eur. Space Agency Spec. Publ., ESA SP–361*, 27–32, 1994.

Bauer, E., S. Hasselmann, K. Hasselmann, and H.C. Graber, Validation and assimilation of Seasat altimeter wave heights using the WAM wave model, *J. Geophys. Res., 97*, 12,671–12,682, 1992.

Booij, N., and L.H. Holthuijsen, Propagation of ocean waves in discrete spectral wave models, *J. Comput. Phys., 68*, 307–326, 1987.

Brüning, C., S. Hasselmann, K. Hasselmann, S. Lehner, and T. Gerling, On the extraction of ocean wave spectra from ERS-1 SAR wave mode image spectra, in *Proceedings of the first ERS-1 Symposium: Space at the Service of our Environment, Eur. Space Agency Spec. Publ., ESA SP-359*, 747–752, 1993.

Brüning, C., S. Hasselmann, K. Hasselmann, S. Lehner, and T. Gerling, A first evaluation of ERS-1 synthetic aperture radar wave mode data, in *The Global Atmosphere and Ocean System (GAOS), 2*, 61-98, 1994.

Cardone, V.J., H.C. Graber, R. Jensen, S. Hasselmann, and M. Caruso, In search of the true wind field in SWADE IOP-1: Ocean wave modelling perspective, in *The Global Atmosphere and Ocean System (GAOS)*, in press, 1995.

de las Heras, M.M., and P.A.E.M. Janssen, Data assimilation with a coupled wind-wave model, *J. Geophys. Res., 97*, 20,261–20,270, 1992.

de Valk, C.F., and C.J. Calkoen, Wave data assimilation in a 3rd generation wave model for the North Sea - An optimal control approach, *Rep. X38*, 62 pp., Delft Hydraul., Delft, Netherlands, 1989.

Fennel, W., and H.U. Lass, *Analytical Theory of Forced Oceanic Waves*, 312 pp., Akademie, Berlin, 1989.

Gerling, T.W., Partitioning sequences and arrays of directional ocean wave spectra into component wave systems, *J. Atmos. and Oceanic Techno., 9*(4), 444–458, 1992.

Hasselmann, S., and K. Hasselmann, The wave model EXACT-NL, in *Ocean Wave Modeling (The SWAMP Group)*, pp. 249–251, Plenum, New York, 1985.

Hasselmann, K., and S. Hasselmann, On the nonlinear mapping of an ocean wave spectrum into a synthetic aperture radar image spectrum and its inversion, *J. Geophys. Res., 96*, 10,713–10,729, 1991.

Hasselmann K., et al., Measurements of wind-wave growth and swell decay during the Joint North Sea Wave Project (JONSWAP), *Dtsch. Hydrogr. Z., 8*(12), suppl. A, 95 pp., 1973.

Hasselmann, K., D.B. Ross, P. Müller, and W. Sell, A parametric wave prediction model, *J. Phys. Oceanogr., 6*, 200–228, 1976.

Hasselmann, K., S. Hasselmann, E. Bauer, C. Brüning, S. Lehner, H.C. Graber, and P. Lionello, Development of a satellite SAR image spectra and altimeter wave height data assimilation system for ERS-1, Rep. 19, 155 pp., Max-Planck-Institut für Meteorologie, Hamburg, Germany, 1988.

Janssen, P.A.E.M., G.J. Komen, and W.J.P. de Voogt, An operational coupled hybrid wave prediction model, *J. Geophys. Res., 89*, 3635–3654, 1984.

Janssen, P.A.E.M., P. Lionello, M. Reistad, and A. Hollingsworth, Hindcasts and data assimilation studies with the WAM model during the Seasat period, *J. Geophys. Res., 94*, 973–993, 1989.

Komen, G.J., Introduction to wave models and assimilation of satellite data in wave models, in The use of satellite data in climate models, Proceedings of the Alpbach Conference, *Eur. Space Agency Spec. Publ., ESA SP 244*, 21–26, 1985.

Komen, G.J., L. Cavaleri, M. Donelan, K. Hasselmann, S. Hasselmann, and P.A.E.M. Janssen, *Dynamics and Modelling of Ocean Waves*, 560 pp., Cambridge Univ. Press, New York, 1994.

Le Dimet, F.X., and O. Talagrand, Variational algorithms for analysis and assimilation of meteorological observations: theoretical aspects, *Tellus Ser. A, 38A*, 97–110, 1986.

Lionello, P., H. Günther, and P.A.E.M. Janssen, Assimilation of altimeter data in a global third-generation wavemodel, *J. Geophys. Res., 97*, 14,453–14,474, 1992.

Marchuk, G.I., *The Numerical Solution of Problems of Atmospheric and Oceanic Dynamics* (in Russian), 387 pp., Gidrometeoizdat, Leningrad, (Engl. transl. by Rainbow Systems Incorpotated, Alexandria, Va., 1974).

Resio, D., and W. Perrie, A numerical study of nonlinear energy fluxes due to wave-wave interactions, 1, Methodology and basic results, *J. Fluid Mech., 223*, 603–629, 1991.

Roach, G.F., *Green's Functions*, 325 pp., Cambridge Univ. Press, New York, 1982.

Romeiser, R., Global validation of the wave model WAM over a 1-year period using Geosat wave height data, *J. Geophys. Res., 98*, 4713–4726, 1993.

Snyder, R.L, F.W. Dobson, J.A. Elliott, and R.B. Long, Array measurements of atmospheric pressure fluctuations above surface gravity waves, *J. Fluid Mech., 102*, 1–59, 1981.

Sobey, R.J., and I.R. Young, Hurricane wind waves - A dis-

crete spectral model, *J. Waterw. Port Coastal Ocean Div. Am. Soc. Civ. Eng., 112*(3), 370–389, 1986.

Thacker, W.C, Three lectures on fitting numerical models to observations, *Rep. GKSS 87/E/65*, 64 pp. , Germany, 1988.

Thomas, J.P., Retrieval of energy spectra from measured data for assimilation into a wave model, *Q. J. R. Meteorol. Soc., 114*, 781–800, 1988.

WAMDI Group, S. Hasselmann et al., The WAM model - A third-generation ocean wave prediction model, *J. Phys. Oceanogr., 18*, 1775– 1810, 1988.

Young, I.R., and G. P. Van Vledder, A review of the central role of nonlinear interactions in wind-wave evolution, *Philos. Trans. R. Soc. London A, 342*, 505–524, 1993.

Young, I.R., S. Hasselmann, and K. Hasselmann, Computations of the response of a wave spectrum to a sudden change in the wind direction, *J. Phys. Oceanogr., 17*, 1317–1338, 1987.

Zakharov, V.E., and N.N. Filonenko, Energy spectrum for stochastic oscillations of the surface of a liquid, *Sov. Phys. Dokl., Engl. transl., 11*, 881-883, 1967.

Zambresky, L., A verification study of the global WAM model December 1987 - November 1988, *Tech. Rep. 63*, 86 pp., Eur. Cent. for Medium-Range Weather Forecasts, Reading, England, 1989.

E. Bauer, Institut für Meereskunde, Universität Hamburg, Troplowitzstraße 7, 22529 Hamburg, Germany. (e-mail: eva.bauer @dkrz.de)

K. Hasselmann and S. Hasselmann, Max-Planck-Institut für Meteorologie, Bundesstraße 56, 20146 Hamburg, Germany.

I. R. Young, Department of Civil and Maritime Engineering, University College, University of New South Wales, Canberra, A.C.T. 2600, Australia

(Received July 27, 1994; revised October 18, 1995;
accepted October 23, 1995.)